Dinitrogen Cleavage

DOI: 10.1002/anie.200801668

Energetics and Mechanism of Dinitrogen Cleavage at a Mononuclear Surface Tantalum Center: A New Way of Dinitrogen Reduction**

*Jun Li and Shuhua Li**

Synthesis of ammonia from dinitrogen (N_2) is one of the most important reactions not only in industry but also in biology.[1,2] In industry, the Haber–Bosch process involves a heterogeneous catalytic reaction in which N_2 and H_2 react on a supported Fe or Ru nanoparticle catalyst at high temperature (350–550 °C) and pressure (150–350 atm). In biology, several types of nitrogenases catalyze the conversion of N_2 to ammonia at ambient temperature and pressure.[3] For decades, enormous efforts have been made to split the robust N≡N bond under mild conditions. Multimetal cooperation was found to be the rule for N_2 activation with a few exceptions, such as molybdenum and tungsten complexes.[4–8] Recently, cleavage of N_2 was achieved at 250 °C and 1 atm by H_2 at the silica-surface-supported mononuclear tantalum centers $[(\equiv SiO)_2TaH]$ and $[(\equiv SiO)_2TaH_3]$ to give the tantalum amido imido product $[(\equiv SiO)_2Ta(=NH)(NH_2)]$.[9] This discovery is the first example of N_2 cleavage at a heterogeneous monometallic center. Reduction of N_2 at a single surface tantalum center may proceed by a mechanism different from that of the Schrock process, in which specific proton and electron sources are required.[7,10] Although some reaction intermediates have been identified experimentally,[9] insight into the energetics and molecular mechanism of this process is still lacking. Therefore, we performed detailed B3LYP DFT[11] calculations to investigate the possible reaction pathways for this novel N_2 reduction reaction.

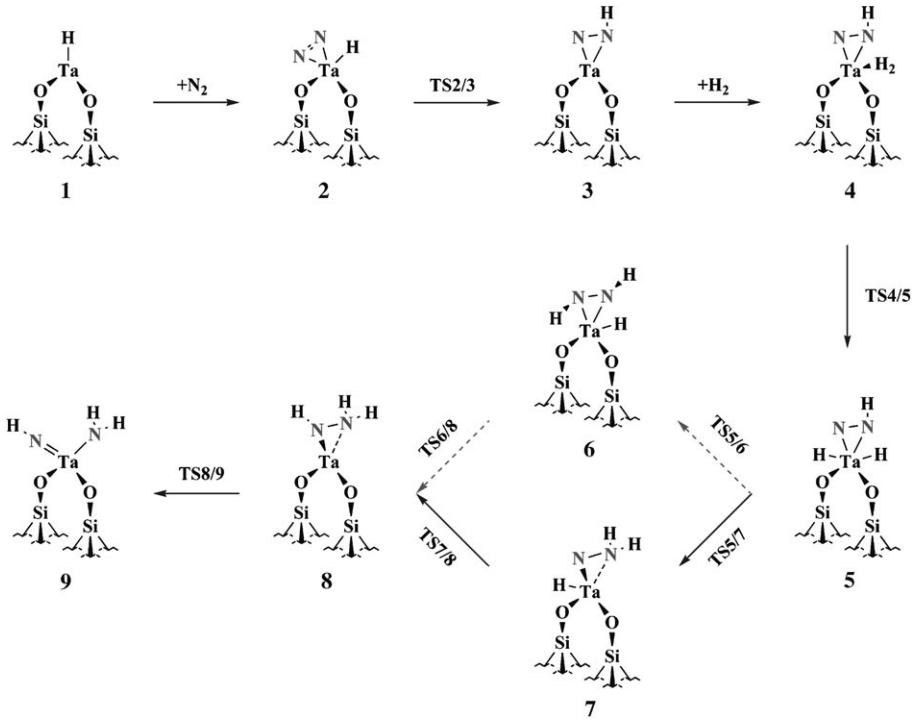

Scheme 1. Schematic structures of all stationary points for the reduction of N_2 by H_2 at a Ta^{III} center.

Using a relatively large cluster model $Si_{14}O_{20}H_{19}Ta$ (see Figure S1, Supporting Information) mimicking the silica-surface-supported tantalum(III) hydride center $[(\equiv SiO)_2TaH]$, we explored the possible pathways for the reduction of N_2 by H_2. The schematic structures of all stationary points are shown in Scheme 1. All calculations were performed with the Gaussian 03 program suite.[12] Computational details are presented in the Supporting Information. The detailed geometrical parameters of the optimized structures are collected in Figure S2 (Supporting Information), and some of them are also shown in Figure 1. For each stationary point, the ground state was determined to be the singlet state (Tables S1 and S2, Supporting Information). In the following, we will focus on the Gibbs energy profile (Figure 2) on the singlet surface, calculated at room temperature and 1 atm.

The starting reactant was chosen to be $[(\equiv SiO)_2TaH]$ (**1**). Coordination of N_2 to **1** proceeds in a side-on mode to form $[(\equiv SiO)_2TaH(N_2)]$ (**2**). The side-on binding of N_2 to **1** is thermodynamically favorable (exergonic by 15.8 kcal mol^{-1}). The subsequent hydride-transfer step leads to diazenido

[*] J. Li, Prof. Dr. S. Li
School of Chemistry and Chemical Engineering
Institute of Theoretical and Computational Chemistry
Key Laboratory of Mesoscopic Chemistry of Ministry of Education
Nanjing University, Jiangsu 210093 (P.R. China)
Fax: (+86) 25-8368-6553
E-mail: shuhua@nju.edu.cn

[**] We gratefully acknowledge financial support by the National Basic Research Program (Grant No. 2004CB719901), the National Natural Science Foundation of China (Grant No. 20625309), and the Chinese Ministry of Education (Grant No. NCET-04-0450).

Supporting information for this article is available on the WWW under http://dx.doi.org/10.1002/anie.200801668.

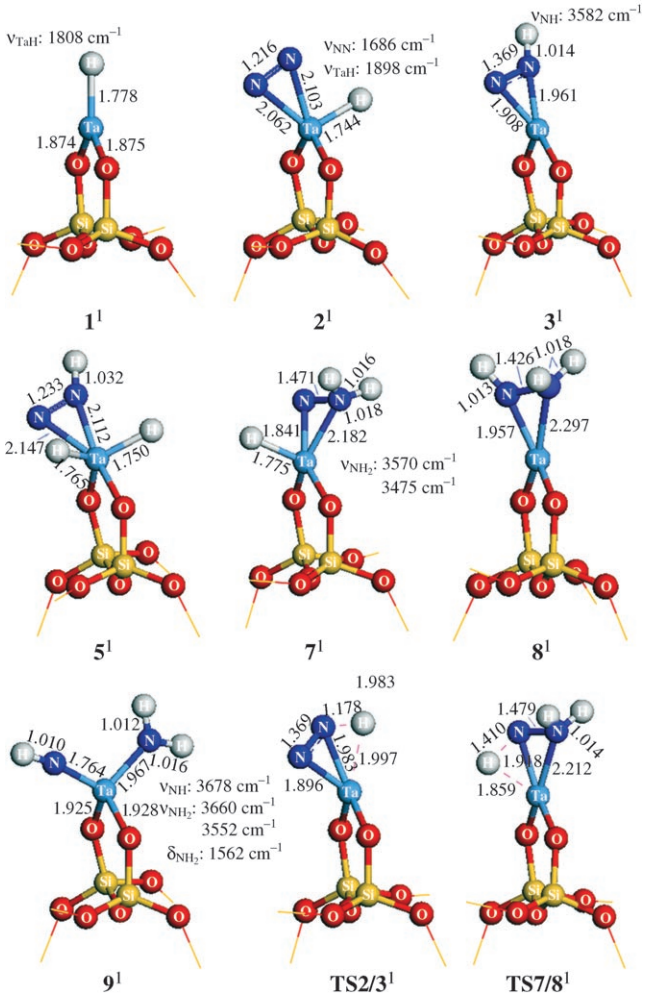

Figure 1. Optimized geometries of some stationary points on the pathway of N_2 reduction at a Ta^{III} center. Bond lengths [Å] and vibrational frequencies (unscaled) are given. The superscript (1) represents the spin multiplicity (singlet).

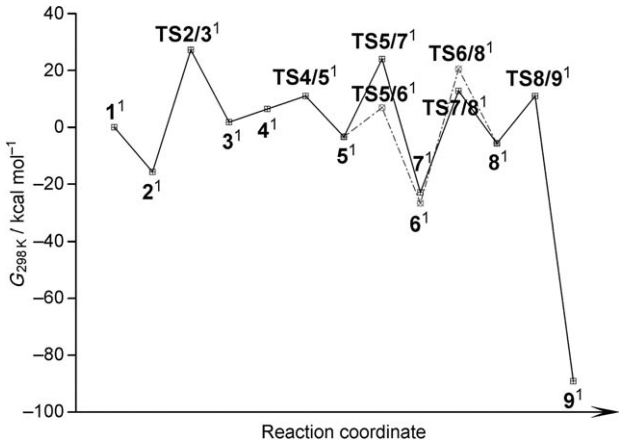

Figure 2. Gibbs energy profile for the reduction of N_2 by H_2 at a single surface Ta^{III} center.

complex $[(\equiv SiO)_2Ta(N_2H)]$ (**3**) via transition state **TS2/3**. As shown in Figure 2, **TS2/3** is the global maximum of the entire Gibbs energy profile and lies 27.2 kcal mol^{-1} above the reactants N_2 and **1**. Next, H_2 coordinates to **3** to form molecular hydrogen complex **4**; this step is endergonic by 5.9 kcal mol^{-1}. Then, oxidative addition of H_2 leads to dihydride species $[(\equiv SiO)_2TaH_2(N_2H)]$ (**5**) via transition state **TS4/5** with a Gibbs energy barrier of 4.5 kcal mol^{-1}. Subsequently, one of the two hydride ligands transfers to the N_2H group by different routes to form intermediate $[(\equiv SiO)_2TaH(N_2H_2)]$ (**6**) or $[(\equiv SiO)_2TaH(NNH_2)]$ (**7**). Then, another hydride transfer converts **6** or **7** to the same hydrazido species $[(\equiv SiO)_2Ta(NHNH_2)]$ (**8**). The route starting with **7** is energetically favorable compared with that starting with **6**. Finally, the N–N bond of the $NHNH_2$ group in **8** is completely broken via transition state **TS8/9** to give the product $[(\equiv SiO)_2Ta(=NH)(NH_2)]$ (**9**). This step is exergonic by 83.9 kcal mol^{-1} and has a Gibbs energy barrier of 16.2 kcal mol^{-1}.

The overall reaction is strongly exergonic by 89.1 kcal mol^{-1}. The two rate-determining steps on the whole pathway are transfer of the first hydride from **2** to **3**, and transfer of the third hydride from **7** to **8**. Although the Gibbs energy barriers from **2** to **TS2/3** (43.0 kcal mol^{-1}) and from **7** to **TS7/8** (35.7 kcal mol^{-1}) are relatively high, these two steps may take place under experimental conditions, possibly by a hydrogen tunneling process.[13] A recent report showed the rearrangement of HCOH to formaldehyde (with an activation barrier of about 30 kcal mol^{-1}) could occur at −260 °C by pure hydrogen tunneling.[14] The results presented herein can give a reasonable explanation on the experimental facts that at 250 °C and 1 atm reduction of N_2 reaches greater than 95 % conversion in three days. In addition, the lowest triplet states of all stationary points are higher in energy than the corresponding singlet states (Tables S1 and S2, Supporting Information), so the reaction is most likely to occur only on the singlet surface. Nevertheless, the singlet–triplet gaps of some species are quite small, and hence their optimized structures in the lowest triplet state are collected in Figure S3 (Supporting Information). For instance, reactant **1** has the smallest singlet–triplet gap (1.0 kcal mol^{-1}). Nevertheless, this value may be underestimated by the B3LYP method, due to the noticeable spin contamination in the singlet state of **1** ($\langle S^2\rangle = 0.52$).

Now we compare the structural and vibrational information obtained from our calculations with those from experiments. An extended X-ray absorption fine structure (EXAFS) study showed that in product **9** the Ta–O distance is 1.93 Å, and the Ta–N distances are 1.81 and 2.04 Å.[9] The calculated values of 1.928, 1.764, and 1.967 Å, respectively, are in good agreement with the experimental values. The computed IR frequencies of **9**, scaled by a recommended factor of 0.9611[15], are 3535 cm^{-1} (ν_{NH}), 3518 and 3414 cm^{-1} (ν_{NH_2}), which can be reasonably assigned to the corresponding experimental results (3500 cm^{-1} for ν_{NH}, 3461 and 3375 cm^{-1} for ν_{NH_2}).[9] Two intermediates were also observed in the experiments: one has the ν_{NN} band at 2280 cm^{-1}, and the other a band at 3407 cm^{-1}, which may correspond to $\nu(N_xH_y)$. Intermediates **2** and **6** may possibly be detectable due to their relative thermal stability (Figure 1). The N–H stretching frequencies in **6** are computed to be 3374 and 3346 cm^{-1} (scaled), close to 3407 cm^{-1}, but the N–N stretching mode

in **2** is calculated to be at 1686 cm^{-1} (not scaled), far from the observed value of 2280 cm^{-1}, which should correspond to a weakly activated N–N bond.

It is of interest whether the side-on coordination of the dinitrogen ligand to Ta^{III} in **2** is more favorable than an end-on coordination. In fact, N_2 can also bind to Ta^{III} in an end-on mode to form a corresponding complex (Figure S5, Supporting Information), but the Gibbs energy of this complex is 2.3 kcal mol^{-1} higher than that of **2**. In the end-on complex, the N–N bond is significantly shorter than in **2** (1.166 vs 1.216 Å). To better understand the side-on binding mode, we consider the HOMO of **2** (Figure 3), which is mainly the in-phase combination of one π* orbital of N_2 and a d orbital of Ta, that is, d→π* backdonation is strong. This strong backdonation significantly activates the N–N bond and leads to a relatively long bond (1.216 Å). Side-on coordination of N_2 was also observed in $[Os(NH_3)_5(N_2)]^{2+}$.[16] Side-on binding of N_2 in **2** is critical for the subsequent hydride-transfer steps.

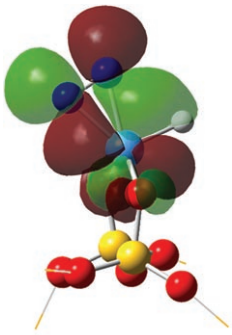

Figure 3. HOMO of $[(\equiv SiO)_2TaH(N_2)]$ (**2**).

In the pathways described above, the Ta^{III} hydride center $[(\equiv SiO)_2TaH]$ was chosen as reactant. Now we consider the Ta^{V} species $[(\equiv SiO)_2TaH_3]$ as reactant. Our calculations show that coordination of N_2 to $[(\equiv SiO)_2TaH_3]$ only leads to an end-on complex with an N–N bond length of 1.105 Å and a Ta–N bond length of 2.456 Å (Figure S6, Supporting Information). Since the bond length in free N_2 is also 1.105 Å, N_2 is very weakly coordinated to the metal center. Binding of N_2 to $[(\equiv SiO)_2TaH_3]$ is endergonic by 6.1 kcal mol^{-1}. The reason for the weak binding is the absence of valence d electrons on the Ta^{V} center for d→π* backdonation.

We also considered the possibility of hydride transfer from the metal to the dinitrogen ligand in the transient $[(\equiv SiO)_2TaH_3(N_2)]$ species. Our geometry optimizations show that the hypothetical intermediate for hydride transfer does not exist (it spontaneously returns to $[(\equiv SiO)_2TaH_3(N_2)]$). From the computed IR frequencies of $[(\equiv SiO)_2TaH_3]$ (1900, 1857, and 1846 cm^{-1}, unscaled), we infer that this trihydride species corresponds to the intermediate observed experimentally to have three IR frequencies of 1880, 1820, and 1760 cm^{-1}.[9] In fact, when H_2 adds to Ta^{III} hydride species $[(\equiv SiO)_2TaH]$ it will spontaneously form $[(\equiv SiO)_2TaH_3]$. The process is exergonic by 28.1 kcal mol^{-1} (at room temperature and 1 atm) without involving any barrier. To shift the above reaction toward the reactants $[(\equiv SiO)_2TaH]$ and H_2, which is the active species for N_2 activation, relatively high temperatures and relatively low dihydrogen partial pressures are required. This result can explain the experimental conditions[9] to some extent. On the other hand, $[(\equiv SiO)_2TaH_3]$ may also transform into $[(\equiv SiO)_2TaH_x]$ and $[\equiv SiH]$ by hydrogen transfer from the Ta atom to an adjacent siloxy bridge.[17]

Since side-on coordination of N_2 to the Ta^{III} center is novel, we wondered whether other transition metals have this property, especially the other group 5 metals Nb and V. Our calculations show that N_2 can also bind side-on to Nb^{III} and V^{III} centers (Figure 4). From the N–N bond lengths in the corresponding optimized structures, the ability of the group 5 metals to activate the N–N bond decreases in the order Ta^{III} > Nb^{III} > V^{III}. The electronic energy of N_2 binding to the metal center is calculated to be 24.5 kcal mol^{-1} for Ta^{III}, 16.5 kcal mol^{-1} for Nb^{III}, and −7.3 kcal mol^{-1} for V^{III}. The negative energy for V^{III} indicates that N_2 may be difficult to bind to the species $[(\equiv SiO)_2VH]$. For the species $[(\equiv SiO)_2NbH(N_2)]$, we also calculated the hydride-transfer transition state (Figure S7, Supporting Information). The activation barrier is 38.9 kcal mol^{-1} (Table S8, Supporting Information), while the corresponding barrier for $[(\equiv SiO)_2TaH(N_2)]$ is 43.0 kcal mol^{-1}. Thus, the Nb^{III} center can be expected to have similar reactivity for activating N_2 to the Ta^{III} center.

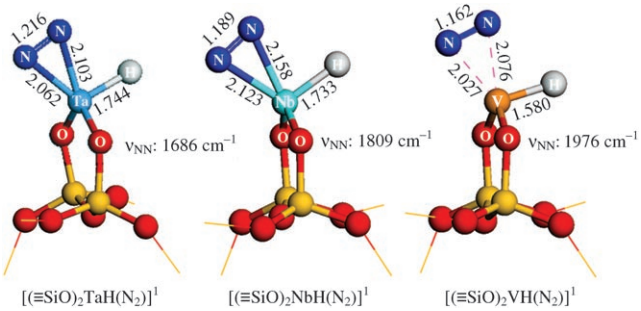

Figure 4. Optimized geometries of $[(\equiv SiO)_2TaH(N_2)]$, $[(\equiv SiO)_2NbH(N_2)]$, and $[(\equiv SiO)_2VH(N_2)]$ with bond lengths [Å].

In summary, the molecular mechanism for the cleavage of N_2 at a mononuclear surface tantalum center has been elucidated by B3LYP calculations. The active species for N_2 reduction is $[(\equiv SiO)_2TaH]$ rather than $[(\equiv SiO)_2TaH_3]$. The rare side-on coordination of N_2 to the Ta^{III} center is critical for the subsequent hydride-transfer steps. Along this pathway, the overall reaction is strongly exergonic, and the two rate-limiting steps are the first and third hydride transfers from the metal to the dinitrogen ligand. The results obtained give reasonable explanations for some experimental findings. Furthermore, our calculations reveal that cleavage of N_2 may also be achieved on a similar mononuclear surface Nb^{III} center.

Received: April 9, 2008
Revised: July 31, 2008
Published online: September 16, 2008

Keywords: coordination modes · density functional calculations · nitrogen fixation · reaction mechanisms · tantalum

[1] M. D. Fryzuk, S. A. Johnson, *Coord. Chem. Rev.* **2000**, *200*, 379–409.
[2] R. R. Schrock, *Proc. Natl. Acad. Sci. USA* **2006**, *103*, 17087.
[3] a) B. K. Burgess, *Chem. Rev.* **1990**, *90*, 1377–1406; b) J. B. Howard, D. C. Rees, *Chem. Rev.* **1996**, *96*, 2965–2982; c) B. K. Burgess, D. J. Lowe, *Chem. Rev.* **1996**, *96*, 2983–3011; d) R. R. Eady, *Chem. Rev.* **1996**, *96*, 3013–3030.

[4] S. Gambarotta, J. Scott, *Angew. Chem.* **2004**, *116*, 5412 – 5422; *Angew. Chem. Int. Ed.* **2004**, *43*, 5298 – 5308.
[5] K. Honkala, A. Hellman, I. N. Remediakis, A. Logadottir, A. Carlsson, S. Dahl, C. H. Christensen, J. K. Nørskov, *Science* **2005**, *307*, 555 – 558.
[6] J. B. Howard, D. C. Rees, *Proc. Natl. Acad. Sci. USA* **2006**, *103*, 17088 – 17093.
[7] D. V. Yandulov, R. R. Schrock, *Science* **2003**, *301*, 76 – 78.
[8] M. Hidai, *Coord. Chem. Rev.* **1999**, *185*, 99 – 108.
[9] P. Avenier, M. Taoufik, A. Lesage, X. Solans-Monfort, A. Baudouin, A. de Mallmann, L. Veyre, J.-M. Basset, O. Eisenstein, L. Emsley, E. A. Quadrelli, *Science* **2007**, *317*, 1056 – 1060.
[10] a) R. R. Schrock, *Acc. Chem. Res.* **2005**, *38*, 955 – 962; b) F. Studt, F. Tuczek, *Angew. Chem.* **2005**, *117*, 5783 – 5787; *Angew. Chem. Int. Ed.* **2005**, *44*, 5639 – 5642; c) M. Reiher, B. Le Guennic, B. Kirchner, *Inorg. Chem.* **2005**, *44*, 9640 – 9642.
[11] a) A. D. Becke, *Phys. Rev. A* **1988**, *38*, 3098 – 3100; b) C. Lee, W. Yang, R. G. Parr, *Phys. Rev. B* **1988**, *37*, 785 – 789; c) A. D. Becke, *J. Chem. Phys.* **1993**, *98*, 5648 – 5652.
[12] Gaussian 03 (Revision B.04): M. J. Frisch et al., see Supporting Information.
[13] a) E. F. Caldin, *Chem. Rev.* **1969**, *69*, 135 – 156; b) A. Kohen, R. Cannio, S. Bartolucci, J. P. Klinman, *Nature* **1999**, *399*, 496 – 499; c) J. Rucker, J. P. Klinman, *J. Am. Chem. Soc.* **1999**, *121*, 1997 – 2006; d) G. Tresadern, J. P. McNamara, M. Mohr, H. Wang, N. A. Burton, I. H. Hillier, *Chem. Phys. Lett.* **2002**, *358*, 489 – 494.
[14] P. R. Schreiner, H. P. Reisenauer, F. C. Pickard IV, A. C. Simmonett, W. D. Allen, E. Mátyus, A. G. Császár, *Nature* **2008**, *453*, 906 – 909; see also: G. Bucher, *Angew. Chem.* **2008**, *120*, 7064; *Angew. Chem. Int. Ed.* **2008**, *47*, 6957.
[15] K. K. Irikura, R. D. Johnson III, R. N. Kacker, *J. Phys. Chem. A* **2005**, *109*, 8430 – 8437.
[16] D. V. Fomitchev, K. A. Bagley, P. Coppens, *J. Am. Chem. Soc.* **2000**, *122*, 532 – 533.
[17] G. Saggio, A. de Mallmann, B. Maunders, M. Taoufik, J. Thivolle-Cazat, J.-M. Basset, *Organometallics* **2002**, *21*, 5167 – 5171.

